JOURNAL OF CATALYSIS 124, 465–476 (1990)

Oxidative Coupling of Methane on Alkali Metal-Promoted Nickel Titanate

II. Kinetic Studies

E. E. MIRO,[1] J. M. SANTAMARIA,[2] AND E. E. WOLF[3]

Chemical Engineering Department, University of Notre Dame, Notre Dame, Indiana 46556

Received November 21, 1989; revised February 6, 1990

The activity, stability, and kinetics of methane oxidative coupling over Li- and Na-promoted nickel–titanate catalysts have been studied. It was found that under the conditions used the C_{2+} yield reached a maximum at 9.7% Li loading and 22% Na loading. Time-on-stream experiments showed that a 1.6% Na-promoted catalyst did not deactivated significantly in 50 h time-on-stream. The 9.7% Li-promoted catalyst and the 22% Na-promoted catalysts lose 15 and 40% yield, respectively, during the same period on stream. Kinetics results obtained under differential conditions resulted in fractional reaction orders and apparent activation energies for methane conversion of 40.9 and 50.5 kcal/mol for the 9.7% $Li/NiTiO_3$ and the 1.6% $Na/NiTiO_3$ catalyst, respectively. The kinetic results are interpreted via a reaction model consisting of a Rideal-redox mechanism for the 9.7% Li-promoted catalyst, and an Eley–Rideal mechanism for the 1.6% Na-promoted catalyst. The reaction pathway proposed agrees well with previous transient measurements of the effect of lattice and adsorbed oxygen on the reaction.

1. INTRODUCTION

The kinetics and mechanism of methane oxidative coupling on a wide variety of catalysts have been the subject of many publications in recent years (*1–5*). It is generally agreed that ethane formation occurs via dehydrogenation of the methane molecule on the catalytic surface, followed by gas-phase coupling of the resulting methyl radicals. Labinger and Ott (*1*) simulated the performance of their Mn/MgO catalyst by combining heterogeneous and gas-phase rate data, and concluded that the role of the surface in hydrocarbon formation is the release of methyl radicals into the gas phase. The types of active site involved in the reaction (*2, 3*) vary with the catalysts and determine the reaction pathway for the formation of the undesired deep oxidation products CO and CO_2 (*4, 5*). Furthermore, since the methane molecule can be activated via adsorbed oxygen, lattice oxygen, or gas-phase oxygen, different kinetic models are expected to be applicable to different catalytic systems.

The oxidation of methyl radicals in nonselective sites competes with the desired coupling reaction; consequently the resulting conversion and selectivity strongly depend on the type of catalysts employed. However, good catalysts for methane oxidative coupling appear to reach a maximum yield near 20% in the majority of cases (*6*). This limitation in yield is probably due to the fact that the main hydrocarbon products, ethane and ethylene, are easily oxidized in the gas phase at the high temperatures currently used (*7*). Thus, new low-temperature catalysts are actively sought, along with different reactor designs in which the contact be-

[1] On leave from INCAPE, Universidad Nacional del Litoral, Sgo.del Estero 2829, 3000 Santa Fe, Argentina.

[2] On leave from the Department of Chemical Engineering, University of Zaragoza, 5009 Zaragoza, Spain.

[3] To whom correspondence should be addressed.

0021-9517/90 $3.00

tween product hydrocarbons and oxygen is minimized (*8*). Thus, it is important to have reliable kinetic expressions which can give an accurate description of the catalytic response to changes in operating conditions for the proper reaction-engineering studies.

Several kinetic studies have been recently published (*4, 5*) in which reaction mechanisms are proposed from experimental steady-state data under differential conditions. In Part I of this work (*9*), we have used transient methods to elucidate the main reaction pathways of methane oxidative coupling over lithium- and sodium-promoted nickel–titanate catalysts. The main reaction steps consisted of interaction of reactants with surface oxygen, very weak methane adsorption, ethane dehydrogenation, and deep oxidation reactions. We have also found that promoting $NiTiO_3$ with either lithium or sodium gives rise to markedly different types of behavior regarding the role of the different oxygen species involved. This work presents steady-state kinetic results for both Li- and Na-promoted $NiTiO_3$ catalysts, which show different reaction rate expressions depending on the type of promoter used. The results are then interpreted via two reaction pathways that are consistent with the previous transient results and that fit the kinetic results fairly well.

EXPERIMENTAL

Catalyst preparation and pretreatment. The catalysts were prepared from the mixed oxide nickel titanate (Alfa products, 99.7%), which was impregnated with a solution of either lithium oxide or sodium carbonate in deionized water. The slurry was heated to 50°C and the water was evaporated with stirring until a dry powder was obtained. Each catalyst was pretreated in flowing air, first at 650°C for 5 h and then at 750°C for 2 h. The amount of alkali metal loading is defined as the initial weight of lithium or sodium divided by the sum of weights of Li_2O or $NaCO_3$ and $NiTiO_3$. The results presented in this work were obtained using catalysts with lithium loadings of 0.5, 5.4, 7.6, 9.7, and 13.8% and sodium loadings of 1.6, 8.7, 14, 22, and 32%. These are denoted in the text by the loading figure preceding Li/$NiTiO_3$ or Na/$NiTiO_3$. Blank runs were also carried out with unpromoted nickel titanate.

Apparatus and procedure. Steady-state kinetic experiments were performed using a single-pass flow reactor made of fused silica with an inside diameter of 0.95 cm and a heated length of 15 cm. The details of this apparatus have been given elsewhere (*9, 11*). The reaction products in the effluent stream were analyzed by a gas chromatograph equipped with Carbosphere and HayeSep Q packed columns as well as TCD/FID detectors.

Experimental conditions were selected in order to minimize gas-phase reactions in all of the runs performed (*7*). Typical operating conditions used to compare the activity of the different catalysts were as follow: atmospheric pressure, 0.25-g loading of catalyst, partial pressure of methane and oxygen divided by the total pressure of 0.4, feed flow rate at ambient conditions of 100 cm^3 min, methane-to-oxygen feed mole ratio of 4, and 750°C. The methane and oxygen conversions and product selectivities were typically compared at 2 h of time-on-stream.

Reaction rate measurements were carried out at low conversions of the limiting reactant, under various temperatures and reactant partial pressures. While conversion comparisons were made under identical operating conditions, the reaction rate measurements at different temperatures were made using different catalyst loadings and flow rates so that differential conditions were maintained. Table 1 summarizes the operating conditions used in the kinetic experiments. Partial pressures of methane and oxygen were varied on both catalysts by changing the flow rate of methane, oxygen, and helium. Partial pressures of methane between 0.07 and 0.21 atm were used while keeping oxygen constant at 0.035 atm, and oxygen partial pressure was varied between 0.014 and 0.068 atm at methane constant pressure of 0.134 atm. Differential conditions were checked by measuring conver-

TABLE 1

Reaction Conditions Used in Kinetic Experiments

	Temp. (°C)	Weight (g)	Flow Rate (cm^3/min)
9.7% $Li/NiTiO_3$	650	0.2	50
	700	0.1	100
	750	0.1	200
1.6% $Na/NiTiO_3$	700	1.0	50
	750	0.25	50
	800	0.25	200

sions at different residence times. Linear behaviors were observed under 10% of limiting reactant conversions.

Since the $1.6Na/NiTiO_3$ catalyst has high stability beyond 50 h of time-on-stream at 800°C, only one sample of catalyst was used at each temperature in the reaction rate measurements. On the other hand, the $9.7Li/NiTiO_3$ catalyst showed a sharp decline in hydrocarbon yield after 8 h of time-on-stream; consequently fresh catalyst samples from the same batch were used in order to start with the same initial activity.

RESULTS

Effect of the alkali-metal loading on activity and selectivity. Unpromoted $NiTiO_3$ is almost inactive for methane oxidative coupling, giving conversions and selectivities similar to those observed for the noncatalyzed gas-phase reaction. However, promotion of $NiTiO_3$ with either Li_2O or Na_2CO_3 greatly increases both methane conversion and product hydrocarbon yield. Figures 1a and 1b display the effect of the promoter weight percent (as calculated from the initial loading in the wet impregnation) on methane conversion (Fig. 1a) and on hydrocarbon selectivity and yield (Fig. 1b) for Li-promoted Ni–titanate catalysts. Figures 2a and 2b show the corresponding results for the Na-promoted catalysts. Figure 1a shows that methane conversion reaches a maximum with lithium loading (at 9.7 wt% of Li), which is more than 47 times higher than that on unpromoted nickel titanate. The hydrocarbon selectivity (Fig. 1b), shows a behavior different from conversion, being approx-

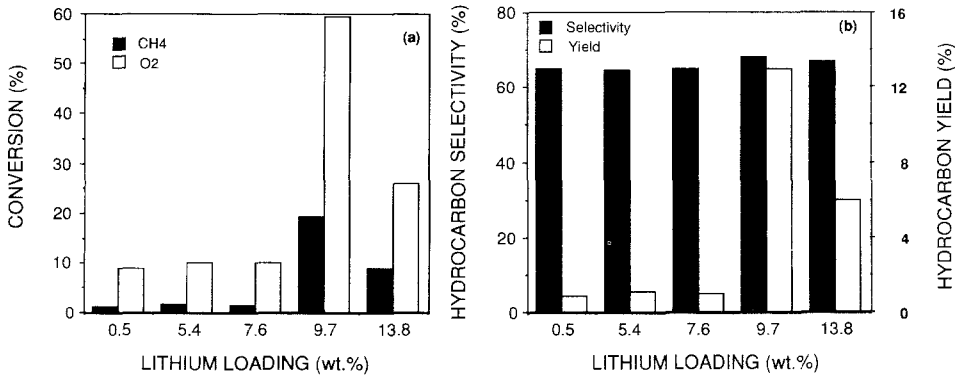

FIG. 1. Comparison of methane and oxygen conversion. (a) Hydrocarbon selectivity and hydrocarbon yield (b) for a series of lithium-promoted nickel–titanate catalysts. The results represent samples taken at 750°C after 2 h time-on-stream with a CH_4/O_2 feed mole ratio of 4, a feed flow rate of 100 cm^3/min, a 0.25-g catalyst sample, and a methane partial pressure of 0.32 atm.

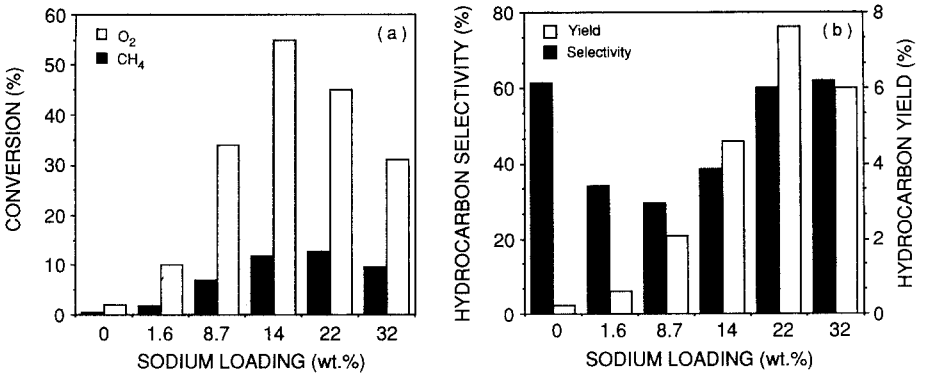

FIG. 2. Comparison of methane and oxygen conversion. (a) Hydrocarbon selectivity and hydrocarbon yield (b) for a series of sodium-promoted nickel–titanate catalysts. The results represent samples taken at 750°C after 2 h time-on-stream with a CH_4/O_2 feed mole ratio of 4, a feed flow rate of 100 cm^3/min, a 0.25-g catalyst sample, and a methane partial pressure of 0.32 atm.

imately constant over a wide range of lithium loadings. Therefore, the yield to C_{2+} hydrocarbons follows the pattern dictated by methane conversion.

The addition of sodium carbonate to nickel titanate also increases methane conversion, which reaches a maximum for 22% sodium loading (Fig. 2a). The conversion versus loading, however, increases more gradually than that in the case of lithium; thus the Na-promoted catalyst presents a wider range of sodium loadings, which give similar conversions. The C_2 hydrocarbon selectivities exhibit a minimum at 8.7% sodium loading, leveling off at higher loadings, which results in a C_2 yield curve with a maximum at 22% sodium loading.

It should be emphasized that the yields reported in Figs. 1 and 2 are not the optimum values—about 23% for the 9.7Li/$NiTiO_3$ and 22Na/$NiTiO_3$ catalysts—attainable with these catalysts. The purpose of the present study however was not to develop more active catalysts, but rather to study the kinetics of the reaction and how it is affected by the nature of the promoter. Thus the conditions chosen in the activity and kinetics studies were selected to minimize gas-phase reactions and to conduct studies under differential reaction conditions rather than to optimize the yield.

Catalyst stability. The stability of the catalysts under reaction conditions was investigated in 50-h runs. Figure 3a shows the change in the yield to produce hydrocarbons and deep oxidation products with time-on-stream for the 9.7Li/$NiTiO_3$ catalyst at 750°C. It can be seen that the catalyst retained its full activity and selectivity for the first 3 h; then, after about 8 h on stream, a sharp decline occurred in the C_{2+} yield, followed by a slower decrease after approximately 25 h. The yield in CO_2 (not shown) was basically unaltered for most of the run.

Figure 3b shows the results of the same experiment for 1.6 and 22% sodium-promoted catalysts at 800°C. The reaction conditions (see figure legend) were chosen to obtain similar yields from both catalysts. The 1.6Na/$NiTiO_3$ catalyst showed a fairly stable behavior during the 50-h experiment, as indicated by the constant 10.5% C_{2+} yield, whereas the yield of the 22Na/$NiTiO_3$ catalyst decreased from 13.7 to 11.7%. The C_{2+} selectivity for both sodium-promoted catalysts remained essentially constant during the 50-h run, at a value of approximately 35% for the 1.6% Na-loaded catalyst and 63% for the 22% Na-loaded catalyst. It should be noted that after the runs with the 9.7Li/$NiTiO_3$ and 22Na/$NiTiO_3$ catalysts, alkali deposits could be observed on the re-

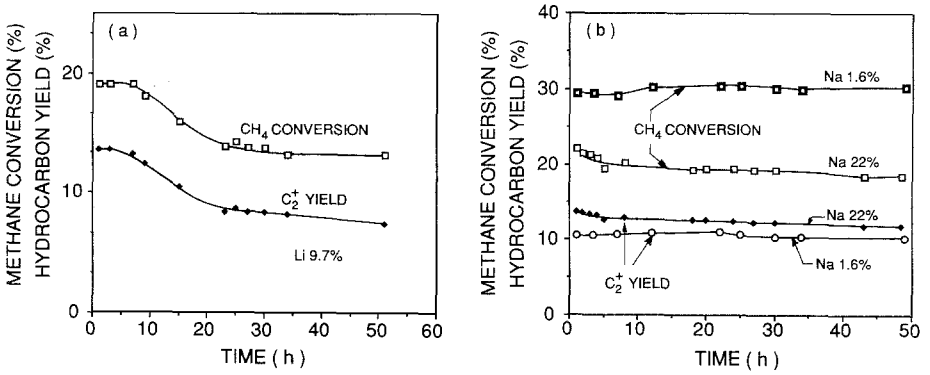

FIG. 3. Effects of time-on-stream; (a) 0.25 g of 9.7% $Li/NiTiO_3$, at 750°C, $CH_4/O_2 = 4$, a total flow rate of 100 cm^3/min, and a methane partial pressure of 0.32 atm; (b) 1.0 g of 1.6% $Na/NiTiO_3$, at 800°C, $CH_4/O_2 = 2$, total flow rate of 100 cm^3/min, and a methane partial pressure of 0.32 atm; and 1.0 g of 22% $Na/NiTiO_3$, at 800°C, $CH_4/O_2 = 4$, a total flow rate of 100 cm^3/min, and a methane partial pressure of 0.32 atm.

actor wall. Although the catalysts with higher sodium loading (14–22%) gave higher hydrocarbon yields and better selectivity than those with lower amounts of sodium, the $1.6Na/NiTiO_3$ catalyst was chosen for the kinetics studies due to its higher stability and lower sodium losses. As for the lithium-loaded catalysts, the $9.7Li/NiTiO_3$ catalyst was selected in view of the results of Part I of this work, in which it was shown that this was the only catalyst in the Li-promoted series exhibiting significant lattice oxygen activity for methane oxidative coupling.

Temperature effects on activity and selectivity. Figures 4a and 4b display the variation in methane conversion and total hydrocarbon selectivity with changes in temperature. With this set of operating conditions, the reactor operated at conversions higher than differential. The trends shown in Fig. 4b for both the $9.7Li/NiTiO_3$ and the $1.6Na/NiTIO_3$ catalysts are similar to other reports presented in the literature, showing improved hydrocarbon selectivity with increasing conversion. However, it can be observed that for the Li-promoted catalyst the selectivity reaches a maximum at approximately 720°C, whereas for the sodium catalyst the selectivity increases continuously between 700 and 800°C. This different behavior is consistent with the interaction of oxygen with the surface as found by transient measurements in Part I of this work (*9*). In the case of the sodium catalyst, the deep oxidation of methyl radicals is the main pathway for CO_x formation, while in the case of the Li-promoted catalyst, the loses in selectivity with temperature are caused mainly by the oxidation of the hydrocarbon products.

Power law kinetics. Figures 5a and 5b shows conversion and selectivity results for the $1.6Na/NiTiO_3$ catalyst vs contact times at 750°C. The change in the product selectivity with contact time shows an almost symmetric distribution between C_2H_6 and C_2H_4 and also between CO and CO_2. This strongly suggest that CO_2 and C_2H_4 are secondary products of the reaction. If the total hydrocarbon and total deep oxidation products are plotted instead of the individual species, an almost constant value is obtained in both cases. The linearity of these plots indicates that differential conversion is attained by operating below 10% oxygen conversion.

The rate data was first fitted to power law kinetics in order to compare the performance of the different catalysts. The power law kinetic parameters were obtained by plotting the logarithm of the reaction rates

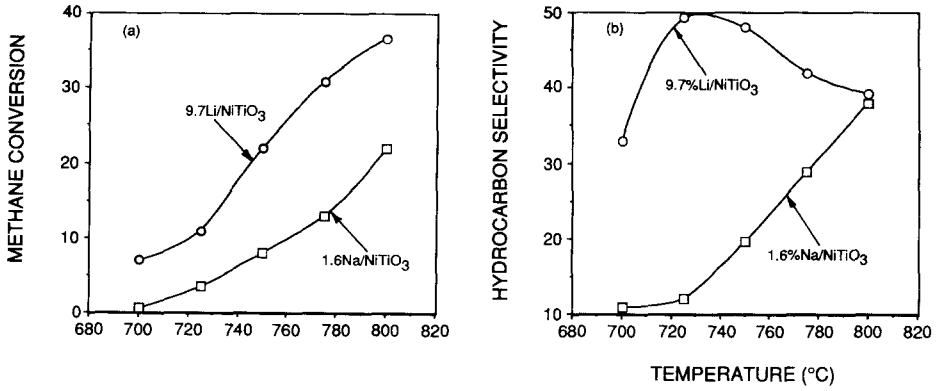

FIG. 4. Temperature effects on methane conversion and higher hydrocarbon selectivity using 0.25 g of 9.7% $Li/NiTiO_3$ catalyst and 1.0 g of 1.6% $Na/NiTiO_3$ catalyst with a feed flow rate of 100 cm^3/min, a CH_4/O_2 feed mole ratio of 2, and a partial pressure of methane of 0.32. (a) Methane conversion and (b) C_{2+} selectivity.

(obtained assuming differential conditions) versus the logarithm of methane and oxygen partial pressures. The apparent activation energies were obtained from Arrhenius plots of methane conversion rates and C_2 hydrocarbon and carbon oxides production rates. Table 2a and 2b summarize the reaction orders and activation energy results obtained with the $9.7Li/NiTiO_3$ and $1.6Na/NiTiO_3$ catalysts, respectively. Due to the differences in the activity of both catalysts, the study of reaction orders on the Li-loaded catalyst was carried out at a lower temperature. It can be observed that fractional reaction orders are obtained for methane conversion in both catalysts. The apparent activation energies obtained from the Arrhenius plots are also given in Tables 2a and 2b. For methane conversion they range from about 40 to 50 kcal/mol over the Li- and Na-loaded catalysts, respectively.

Reaction pathways and associated kinetics. In previous work in our laboratory (*11–12*) we have proposed (*11*) a reaction pathway in which, at integral conversion, the main restriction for the hydrocarbon

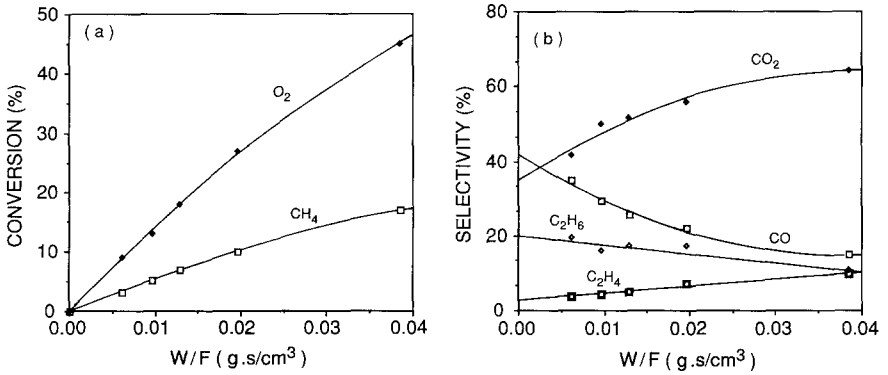

FIG. 5. The effect of contact time on CH_4 and O_2 conversions (a) and on product selectivities (b) at 750°C using a 1.6% $Na/NiTiO_3$ catalyst with a feed mole ratio of 2, a 1.0-g sample, and a methane partial pressure of 0.134 atm.

TABLE 2a

Power Law Kinetic Parameters for 9.7% $Li/NiTiO_3$: Apparent Reaction Orders and Activation Energies

	Reaction orders						E
	650°C		700°C		750°C		
R_j	CH_4	O_2	CH_4	O_2	CH_4	O_2	(kcal/mol)
CH_4	0.7	0.2	0.7	0.2	1.0	0.4	40.9
C_2	1.0	0.0	1.1	0.0	1.2	0.2	46.2
CO_x	0.5	0.3	0.3	0.6	0.4	0.7	34.7

TABLE 2b

Power Law Kinetic Parameters for 1.6% $Na/NiTiO_3$: Apparent Reaction Orders and Activation Energies

	Reaction orders						E
	700°C		750°C		800°C		
R_j	CH_4	O_2	CH_4	O_2	CH_4	O_2	(kcal/mol)
CH_4	0.7	0.4	0.9	0.7	0.8	0.6	50.5
C_2	1.2	−0.3	1.1	0.1	1.0	0.4	59.4
CO_x	0.6	0.5	0.5	1.2	0.6	1.0	40.0

product yield was the oxidation of C_2 hydrocarbons in the gas phase. The Li/TiO_2 catalyst used in the said study (*11*) activated methane to form methyl radicals via reaction with adsorbed oxygen species, while lattice oxygen showed only nonselective activity.

In Part I of this work (*9*), we obtained the following results over lithium- and sodium-loaded nickel titanates via transient experiments and isotopic tracers (*9*):(a) $^{13}CH_4$ tracing experiments indicated that the concentration of long-lived adsorbed methane intermediates was such that it could not be differentiated from the retention time of Ar. These results suggest that methane reacts mainly via collisions from the gas phase with surface oxygen which abstract hydrogen and form methyl radicals. (b) Trace oxygen monitoring, out-of-phase methane and oxygen steps, pulse experiments with different amounts of oxygen, and isotopic tracing experiments showed that on the $9.7Li/NiTiO_3$ catalysts, methane reacts with oxygen stored in the lattice. The mobility of the lattice oxygen from the bulk of this catalyst is high enough to quickly restore the oxygen depleted near the surface. When the same experiments were performed over the $1.6Na/NiTiO_3$ catalysts, or over Na-promoted catalysts with higher Na loadings, the results indicated that there was no participation of lattice oxygen. Instead, on the sodium-promoted catalysts, the reaction takes place mainly via adsorbed oxygen.

The above results indicate that on the lithium- and sodium-promoted catalysts methane interacts with surface oxygen in both cases. In the case of the Li-promoted catalyst, surface oxygen is supplied from the lattice, thus constituting a redox-type mechanism, whereas in the case of the Na-promoted catalysts methane reacts mainly via adsorbed oxygen without utilization of lattice oxygen. The corresponding representation of both pathways is as follows. For Li,

$$\tfrac{1}{2}O_2 + S \xrightarrow{k_1} (O) \qquad \text{(i)}$$

$$CH_4 + (O) \xrightarrow{k_2} \cdot CH_3 + \cdot OH_{(a)} + S, \qquad \text{(ii)}$$

where S denotes an active site and (O) denotes lattice oxygen on the catalyst surface. Assuming steady state for the active oxygen species and in agreement with the previous work of Asami *et al.* (*3*) and Iwamatsu and Aika (*4*), in which the adsorption rate of oxygen is assumed to be proportional to the oxygen pressure and the concentration of the active site, and step (ii) is first order in methane pressure, we obtain the linearized equation

$$\frac{P_{O_2}}{R_{CH_4}} = \frac{1}{k_1} + \frac{P_{O_2}}{k_2 P_{CH_4}}, \qquad (1)$$

which is similar to the expression obtained assuming the well-known Mars van Krevelen redox mechanism.

For Na,

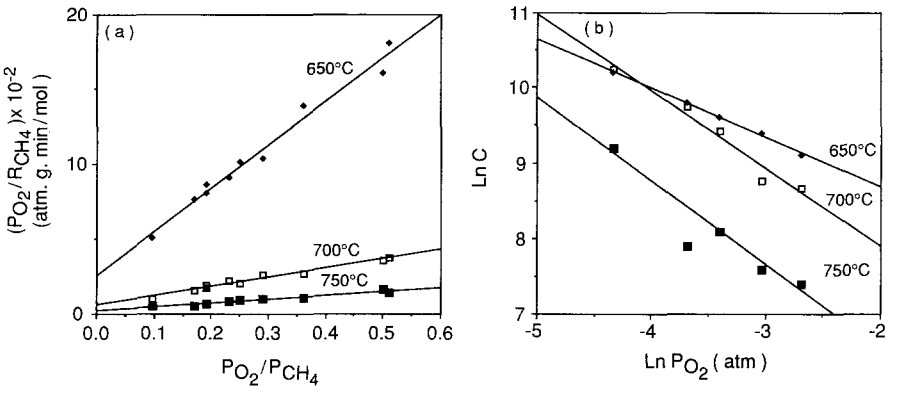

FIG. 6. (a) Reactant pressure ratio (P_{O_2}/P_{CH_4}) dependence for P_{O_2}/R_{CH_4} over a 9.7% Li/NiTiO$_3$ catalyst at 700, 750, and 800°C; (b) ln C as a function of ln P_{O_2} over a 9.7% Li/NiTiO$_3$ catalyst at 700, 750, and 800°C.

$$O_2 + \text{site} \overset{K_{ads}}{\leftrightarrows} (O_2)_{ads}$$

$$CH_4 + (O_2)_{ads} \overset{k_1}{\rightarrow} \cdot CH_3 + \cdot HO_2 + \text{site}, \qquad \text{(ii')}$$

where $(O_2)_{ads}$ represents adsorbed molecular oxygen. The Eley–Rideal mechanism leads to the following expression for the methane reaction rate:

$$R_{CH_4} = \frac{k_1 K P_{O_2} P_{CH_4}}{(1 + K P_{O_2})}. \qquad (2)$$

The same steps, consisting of the recombination of methyl radicals in the gas phase to yield C_2H_6 and oxidation of methyl radicals with gas-phase or surface oxygen, are assumed for both catalysts. Since the detailed mechanism of the methyl radical oxidation is unknown, we propose the use of an undefined stoichiometric coefficient for the oxygen ($x/2$), as previously introduced by Iwamatsu and Aika (*4*).

$$\cdot CH_3 + \frac{x}{2} O_2 \overset{k_3}{\rightarrow} CO, CO_2 \qquad \text{(iii)}$$

$$2 \cdot CH_3 \overset{k_4}{\rightarrow} C_2H_6, \qquad \text{(iv)}$$

which leads to the following expression for both mechanisms

$$\ln \frac{R_2}{R_1^2} = \ln \left(\frac{k_4}{k_3^2}\right) - x \ln P_{O_2}, \qquad (3)$$

where R_1 and R_2 are the rates of CO_x and C_2 formation, respectively.

TABLE 3a

Redox Mechanism Parameters for 9.7% Li/NiTiO$_3$ Catalyst[a]

	650°C	700°C	750°C
k_1	3.9×10^{-3}	1.6×10^{-2}	4.0×10^{-2}
k_2	3.4×10^{-4}	2.0×10^{-3}	3.9×10^{-3}
k_3^2/k_4	6.3×10^{-4}	2.9×10^{-3}	1.2×10^{-2}
x	0.7	1.0	1.0

[a] Units: k_1 and k_2 (gmol/atm g min); k_3^2/k_4 (gmol/atm^x g min).

TABLE 3b

Eley–Rideal Mechanism Parameters for 1.6% Na/NiTiO$_3$ Catalyst[b]

	700°C	750°C	800°C
k_1	9.8×10^{-5}	6.1×10^{-4}	3.5×10^{-3}
K	26.0	9.4	4.4
k_3^2/k_4	9.5×10^{-3}	2.3×10^{-2}	1.1×10^{-2}
x	1.3	1.9	1.7

[b] Units: k_1 (gmol/g min atm); k_3^2/k_4 (gmol/atm^x g min); K (1/atm).

Figure 6a shows a plot of P_{O_2}/R_{CH_4} versus P_{O_2}/P_{CH_4}, and Fig. 6b a plot of ln (R_2/R_1) vs ln P_{O_2} for the kinetic data obtained on the 9.7Li/$NiTiO_3$ catalyst at 650, 700, and 750°C. The corresponding values of the rate constants k_1, k_2, and the ratio k_4/k_3^2 as well as x are given in Table 3a. Since $k_2 \ll k_1$, it can also be concluded that the reaction velocity of the oxidation step is much faster than that corresponding to the reduction step, which indicates that the catalytic surface remains mostly oxidized under steady-state reaction conditions.

Equations (1) and (2) were used to fit the kinetic results obtained with the 1.6Na/$NiTiO_3$ catalyst at 700, 750, and 800°C (Fig. 7). A very good agreement was obtained when the data were fitted to the expression representing the Eley–Rideal mechanism (Eq. (2)); this is consistent with the transient results, which indicated that on this catalyst methane activation occurred via adsorbed oxygen rather than by a lattice-activated reaction (Figs. 7a and 7b). Conversely, when the data are fitted to the Rideal-redox expression (Eq. 1) the agreement is not satisfactory. Not only are the data scattered when plotted in the terms involved in Eq. (1), but also the data obtained by varying the oxygen partial pressure at a fixed methane partial pressure clearly follow a trend different from those obtained with different methane partial pressures at a fixed oxygen partial pressure (Fig. 7c).

Equation (3), which is valid for both mechanisms, fits satisfactorily the data obtained with the 1.6Na/$NiTiO_3$ catalyst (not shown). The constants obtained using the Eley–Rideal mechanism for this catalyst are summarized in Table 3b, along with the corresponding values of the stoichiometric coefficient x.

DISCUSSION

In this paper we present the effects of promoter loading, stability, and kinetics on Li- and Na-promoted Ni–titanate catalysts. Furthermore, it is shown that kinetic expressions based on a reaction pathway consistent with previous transient and isotopic tracer results can reflect the experimental kinetic results obtained.

The observation of a maximum yield with promoter loading has also been made for other supports, namely Li/TiO_2 and Li/$2TiO_2 \cdot La_2O_3$ (*12*). The maximum yield is the combined effect of increases in conversion and selectivity with loading, followed by a decrease in conversion at the highest loading used. It should be noted that the conversion results reported in our work have been obtained in more concentrated feeds than those used in the majority of the work reported in the literature, which have been obtained with rather dilute feeds. Under our conditions, catalysts which exhibit high yields under dilute streams give rather low conversions (*7*). Conversely, the catalysts studied in this work will give yields of about 23%, if studied under dilute conditions. However, the conditions used were not selected to optimize the yield but to conduct kinetic studies under the appropriate conditions. Another point that must be emphasized is that the loadings used are in excess of monolayer coverage and that the reduction in conversion seen at the high loadings is the result of a decrease in surface area (*11*). Thus, as shown previously (*9*) via XRD and XPS, the effect of loading observed in these complex catalysts is likely associated with the formation of mixed oxide phases containing the active sites for the adsorption of surface oxygen or the storage of lattice oxygen. This explains the sensitivity of the results to the promoter–support combination.

Although, in the 9.7Li/$NiTiO_3$ catalyst, methane reacted with lattice oxygen, we did not find a correlation between the extent of participation of lattice oxygen with Li loading. So, clearly, not only is the type of promoter involved relevant in the participation of lattice oxygen, but its chemical composition is also important. Furthermore, the type of support used is also important, as shown by the results reported by Gaffney *et al.* (*13*), who showed that their Na-promoted

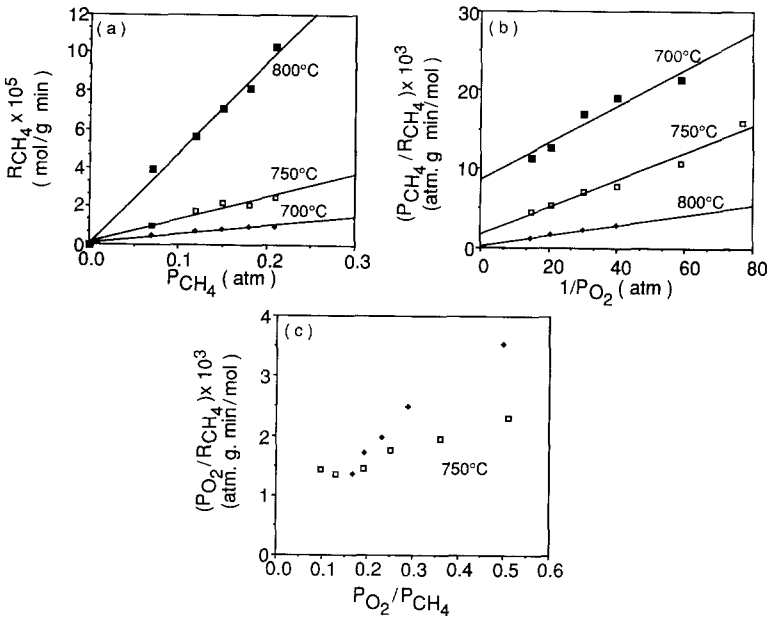

FIG. 7. (a) Methane reaction rate as a function of methane partial pressure over a 1.6% $Na/NiTiO_3$ at 700, 750, and 800°C. (b) Oxygen pressure dependence for P_{CH_4}/R_{CH_4} over a 1.6% $Na/NiTiO_3$ catalyst at 700, 750, and 800°C. (c) Reactant pressure ratio (P_{O_2}/P_{CH_4}) dependence for P_{O_2}/R_{CH_4} over a 1.6% $Na/NiTiO_3$ catalyst at 700, 750, and 800°C.

Pr_6O_{11} activates methane via a redox mechanism. Similarly, Iwamatsu and Aika (*4*), reported that the Rideal-redox mechanism fits their data for the Na-promoted MgO catalysts, while we found that in our $Na/NiTiO_3$ catalysts the Na promoter did not follow a redox mechanism involving lattice oxygen. Studies are underway in our laboratory to determine the factors controlling the participation of lattice oxygen in methane oxidative coupling. Some preliminary results on peroskavite materials which have sufficiently high mobility of lattice oxygen to exhibit ionic conductance showed that these solids are good methane combustion catalysts with no hydrocarbon selectivity. Thus, not only the extent of lattice oxygen is relevant but also its mobility appears to be important to the selective oxidation of methane.

Another observation reported in this work is the different stability to deactivation, which is a function of the promoter and its loading. Deactivation is related to the loss of active sites, which is related to the promoter loading. While promoter losses occurred in Li- and Na-promoted catalysts, they resulted in a decrease in conversion in the Li-promoted catalyst, while not affecting significantly the Na-promoted catalyst. This can be explained by considering that in the Li-promoted catalyst a change from 9.7 to 7.7% loading resulted in a 11.4% difference in hydrocarbon yield. This sensitivity to loading is related to the capacity of the $9.7Li/NiTiO_3$ catalyst to activate methane via lattice oxygen, whereas lower loadings do not exhibit such a property. Thus, as Li losses occur, the capacity to utilize lattice oxygen also decreases, resulting in catalyst deactivation.

The $Na/NiTiO_3$ catalysts were relatively stable to deactivation in the period studied, even though Na losses are visible on the walls at the reactor outlet. This effect can be rationalized in part by the lower sensitiv-

ity of the yield to loading exhibited by this catalyst (Fig. 2). Na losses do not affect the concentration of the sites required for the adsorption of surface oxygen. XPS results (*9*) show that the surface composition of Na on the 22Na/NiTiO3 catalyst remained almost constant after the 50-h time-on-stream run. Apparently, since this catalyst loading is in excess of monolayer coverage, as Na losses occur new sites are exposed or Na migrates from the bulk or other inactive phases onto the surface to form the active sites, so that its concentration remains constant. Eventually, as Na is depleted from the surface, the activity will begin decreasing.

An important relation demonstrated in this work is the relevance of kinetic analysis based on reaction pathway considerations versus that obtained from power law kinetics. The results obtained from the latter rate expressions indicate that the reaction orders are fractional but they are not consistent with the reaction pathway established in Part I of this work (*9*). On the other hand, the kinetic expressions derived from the reaction pathway for oxygen utilization by either catalyst, previously demonstrated in Part I (*9*), fit nicely the experimental results obtained. While the consistency of results is reassuring, it must be noted that several assumptions are involved in the derivation of the corresponding rate expression, which do not represent true elementary reaction steps.

In the case of the Rideal-redox mechanism, an oxygen molecule is assumed to be adsorbed onto one site to yield lattice oxygen. Clearly this is not an elementary step, for to be so oxygen must be adsorbed dissociatively onto two surface sites and then diffuse into the bulk lattice vacancies. An elementary step would require a second-order adsorption process and it would also involve a step for the migration of the surface oxygen into the lattice as well as the opposite process to resupply oxygen from the bulk to the surface. One can rationalize the adequacy of the fit between experimental data and the derived rate expressions by assuming that the omitted steps are sufficiently fast that they do not control the rate of lattice oxygen migration and storage. The surface reduction step also does not specify the fate of the OH radical left on the surface, but it must be assumed that its termination does not affect the reaction. Iwamatsu and Aika (*4*) used the same assumptions in their Rideal-redox mechanism, which is indeed a variation of the Mars and Van Krevelen redox mechanism. The kinetic rate constants resulting from the Rideal-redox mechanism (Table 3) indicate that the surface oxidation rate constant is an order of magnitude higher than the reduction rate constant, which suggests that the surface remains oxidized mainly during the cofed operation of the reactor. Otherwise the formation of metallic Ni will lead to a nonselective catalyst.

Regarding the Eley–Rideal kinetics, it is assumed that molecular oxygen interacts nondissociatively but reversibly with a single active site. This species then reacts with gas-phase methane to form methyl radicals in the gas phase and an hydroperoxy radical. The fate of the latter radical is also left unspecified, but these radicals are known to be quite important in activating gas-phase methane (*7*). One can rationalize the latter omission by assuming that termination of this radical takes place without involving methane or the reaction products.

The activation energies for the oxidation of the $Li/NiTiO_3$ catalysts are 44.0 and 46.3 kcal/mol, respectively. Assuming that the recombination of methyl radicals is not an activated process, one can estimate (from k_3) that the activation energies for the oxidation of methyl radicals are 27.3 and 2 kcal/mol respectively for the $9.7Li/NiTiO_3$ and the $1.6Na/NiTiO_3$ catalysts. The dissimilarity of these values also suggests that the third step is quite different for these two catalysts. At low conversion, the deep oxidation products are presumably produced by the decomposition of methylperoxide radicals which can take place via the gas phase or, most likely, on the surface (*14, 15*), and thus this step is sensitive to the type

of sites available on the surface. Furthermore the values of the stoichiometric coefficient (x) are also different for Li- and Na-promoted catalysts, which again suggests that the pathways for deep oxidation are different for both catalysts.

CONCLUSIONS

The results presented in this work, as well as in the previous paper in this series (*9*), are useful in understanding the importance of catalyst promoters in the oxidative coupling of methane. Thus, evidence has been presented that substantial changes in the interaction of methane with the different oxygen species present in the system can be induced by changing the alkali metal promoter and its loading on the same starting material ($NiTiO_3$). It is shown that changes in the interaction of oxygen can be related to the experimental kinetic results via reaction pathways that are consistent with previous transient results.

ACKNOWLEDGMENTS

The financial support of Amoco Research Laboratories (Naperville IL) is gratefully acknowledged. One of the authors (J.M.S.) is grateful to the Direccion General de Investigacion Cientifica y Tecnica, Spain, for support as a Visiting Scholar.

REFERENCES

1. Labinger, J. A., and Ott, K. C., *J. Phys. Chem.* **91,** 2682 (1987).
2. Ito, T., Wang, J.-X., Lin, C.-H., and Lunsford, J. H., *J. Amer. Chem. Soc.* **107,** 5062 (1985).
3. Asami, K., Shikada, T., Fujimoto, K., and Tominaga, H., *Ind. Eng. Chem. Res.* **26,** 2348 (1987).
4. Iwamatsu, E., and Aika, K.-I., *J. Catal.* **117,** 416 (1989).
5. Ross, J. A., Korf, S. J., Veehof, R. H. J., Van Ommen, J. G., and Ross, J. R. H., *Appl. Catal.* **52**(1–2), 147 (1989).
6. Lee, J. S. and Oyama, S. T., *Catal. Rev. Sci. Eng.* **30**(2), 249 (1988).
7. Lane, G. S., and Wolf, E. E., *J. Catal.* **113,** 144 (1988).
8. Omata, K., Hashimoto, S., Tominaga, H., and Fujimoto, K., *Appl. Catal.* **52,** L1 (1989).
9. Miro, E. E., Santamaria, J. M., and Wolf, E. E., *J. Catal.* **124,** 451 (1990).
10. Lane, G. S., Kalenik, Z., and Wolf, E. E., *Appl. Catal.* **53,** 183 (1989).
11. Lane, G. S., Moro, E. E., and Wolf, E. E., *J. Catal.* **119,** 161 (1989).
12. Miro, E. E., Kalenik, Z., Santamaria, J., and Wolf, E. E., *Catal. Today*, **6,** 511 (1990).
13. Gaffney, A. M., Jones, C. A., Leonard, J. J., and Sofranko, J. A., *J. Catal.* **114,** 422 (1988).
14. Sinev, M. Y., Korchak, V. N., and Krylov, O. V., *Kinet. Katal.* **28,** 1376 (1987).
15. Deboy, J. M., and Hicks, R. F., *J. Catal.* **113,** 517 (1988).